J Mol Model (2002) 8:314–326
DOI 10.1007/s00894-002-0100-2

ORIGINAL PAPER

Ahmed S. Shalabi

F^+ tunable laser activity and interaction of atomic halogens (F, Cl and Br) at the low coordinated surface sites of SrO

Ab initio and DFT calculations

Received: 21 May 2002 / Accepted: 17 September 2002 / Published online: 25 October 2002

Abstract The twofold potential of F^+ color centers at the low coordinated surfaces of SrO for providing tunable laser activity and adsorption properties for atomic halogens (F, Cl and Br) has been investigated using ab initio electronic structure calculations. SrO clusters of variable sizes were embedded in simulated Coulomb fields that closely approximate the Madelung fields of the host surfaces and the nearest neighbor ions to F^+ were allowed to relax to equilibrium. Based on Stokes shifted optical transition bands and horizontal shifts along the configuration coordinate diagrams, the F^+ laser activity was found to decrease as the coordination number of the surface ions decreases from 5 (flat) to 4 (edge) to 3 (corner). An attempt has been made to explain this result in terms of Madelung potentials and optical–optical conversion efficiencies. All relaxed excited states are deep below the conduction bands of the perfect ground states, implying that F^+ is a laser-suitable defect. The most laser active flat surface is the least probable for relaxed excited state orientational destruction of F^+. The excited state at the edge has the highest energy, implying exciton (energy) transfer to the flat and edge sites. F^+ relaxation and defect-formation energies increase with increasing surface coordination number. The Glasner–Tompkins relation between the fundamental optical absorption of F^+ in solids and the fundamental absorption of the host crystals can be generalized to include the low coordinated surfaces of SrO. The F^+ color center changes the nature of halogen–surface interaction (adsorption energies) from physical adsorption to chemical adsorption. The halogen–surface interactions increase with increasing electronegativity of the halogen. The calculated adsorption energies can be explained in terms of surface electrostatic potentials, and the covalent spin pairing mechanism plays a dominant role in determining adsorbate–substrate interactions.

A.S. Shalabi (✉)
Department of Chemistry, Faculty of Science, Benha University,
P.O. Box 13518, Benha, Egypt
e-mail: asshalabi@hotmail.com
Tel.: +20-10-5211-681, Fax: +20-2-4188-738

Keywords F^+ laser · Halogen–surface interactions · SrO · Ab initio

Introduction

Modeling of solid state processes has reached the stage at which applications to solid state lasers would be fruitful. Theoretical modeling is an especially powerful tool in searching for new materials. Investigations of host crystals that can be operated as tunable solid state lasers have stimulated considerable interest in the scientific community. Frequent host crystals are rock-salt oxides, perovskites, garnets, beryls, alkali halides, fluoroperovskites, elpasolites, and fluorites. Usual impurities are the ions of transition metals (mostly of the first series); ns^2 elements; lanthanides, which usually enter the host crystal as substitutional impurities; or alkali metal ions, which give rise to laser-active color centers. [1, 2] The first visible laser, using ruby, uses chromium as the active element doped in aluminum oxide. Other examples of vibronic lasers in oxide materials are Al_2O_3:Ti^+, $GdScGe(SiO_4)_3$:Cr^+, MgO:Ni^{2+} and CaO:F^+. [3] For rock-salt oxides, the electron–hole centers such as F^+, are probably the least studied theoretically. [4] Color-center lasers based on F^+ defects in oxides have produced lasers covering the 0.8–3.65 μm wavelength range with high outputs. However, at the present stage of development, many of the crystals have a drawback in that the effects of excitation encourage charge transfer and defect migration, so that the laser performance degrades. [3]

As far as tunable laser applications are concerned, electron–phonon coupling provides the most important property of broadened Stokes shifted optical transition bands between absorption and emission and an almost ideal four energy level scheme. [5] The electrons associated with a defect interact strongly with the surrounding vibrating crystal ions, resulting in optical transitions, which are allowed in a broad band around the defect-specific central transitions. All color-center lasers real-

ized so far are based on electronic defects and a laser-suitable defect should have the following properties: (1) one-electron center; (2) compact electronic states; and (3) relaxed excited state (RES) deep below the conduction band. [5] The optical properties of the low coordinated surfaces of MgO have been reported by Levine [6] and by Garrone and Zecchina. [7] Quantum mechanical calculations have been performed by Kotomin et al. [8] and by Eglitis et al. [9] for electron–hole centers in MgO, and by Shluger et al. [10] for the excited states at the low coordinated (001) plane surface of MgO. More recently, Shluger et al. [11] reported a dramatic dependence of the calculated optical absorption and luminescence energies of low coordinated sites at the surfaces and nanoclusters of MgO on the oxygen coordination. Experimentally, several optical features have been attributed to the presence of these sites. [12] However, ab initio evaluation of laser performance at the surfaces of rock-salt oxides is still lacking, and until recently the potential of F^+ color centers (an anion vacancy trapping an electron in oxides) for useful laser action at the low coordinated surfaces of SrO has not been paid enough theoretical attention. We have therefore made an attempt to evaluate the F^+ laser performance at the low coordinated surfaces of SrO, in addition to some related properties such as the RES orientational destruction of the center, relaxation and formation energies, exciton (energy) transfer, Glasner–Tompkins relation and the relative positions of the relaxed excited states with respect to the conduction band of the perfect crystal using ab initio methods of molecular electronic structure calculations.

As far as adsorbate–substrate interactions are concerned, metal oxide interfaces are known to be of considerable practical and technological importance. [13, 14] As a model substrate, the MgO (001) surface is probably the most widely used for both experimental and theoretical studies. [15, 16, 17, 18] The simplicity of the MgO cubic structure and the reported lack of strong structural modifications upon metal deposition reduce the computational effort of numerical modeling. However, less theoretical attention has been paid to the other rock-salt oxide surfaces, and for metal oxide interfaces the relative importance of different energetic contributions to the adhesion is rather poorly known. Moreover, understanding the nature of adsorbate–substrate interactions is of great importance in fields such as catalysis, corrosion, gas sensors, and microelectronics. Adsorbate–substrate interactions result from the tendency of the adsorbate valence electrons to interact with the available substrate electrons. This interaction can be expected to play a major role if a small energy gap exists between the adsorbate and the substrate surface, or if the adsorbate has an open shell electronic configuration where covalent spin pairing occurs with the substrate single electron. Studies of interactions at the (001) surface of SrO prove the validity of models at rock-salt oxides and expand the scope of our physical understanding of the surface-defect properties of insulators. However, very little is yet known about the interaction of atomic halogens F, Cl, and Br at SrO low coordinated surfaces. We have therefore performed a fairly extensive set of ab initio calculations to shed light on the effects of F^+ color centers on the interaction of F, Cl, and Br at the flat surface of SrO as well as the relative roles of energy gaps and covalent spin pairing in the course of adsorbate–substrate interactions. To our knowledge, theoretical modeling of SrO surface halogenation is still lacking.

Methods

Crystal simulation

There are several methods to simulate crystals, either by finite or infinite systems. In the case of finite systems, only local portions of the crystal are considered. For such an approach, clusters of varying sizes are suitable approximations. Here one must distinguish between free clusters, saturated clusters, and embedded clusters. Free clusters are simply parts of the bulk, and their simulations should work best if the structures of the stable clusters and of the bulk are very similar. Since free clusters have rather large closed surfaces due to the many surface sections around the outer cluster atoms, it seems advantageous to saturate the free valencies at all sites that are not supposed to represent the real crystal. This saturation can be achieved by simulation with real atoms or pseudoatoms. Alternatively, the free cluster can be embedded in an electric field of point charges, which are an approximation for the rest of the bulk. In the case of infinite systems, the influence of the bulk can be taken into account by point charges rather than by atoms. This procedure can be used for ionic crystals with atoms of alternating charges. An approach that preserves the transitional invariance of ideal crystals is the primitive unit cell (PUC) method. This method uses Bloch functions with many wave vectors, k, to account for the transitional periodicity of the unit cell. However, instead of using complex wavefunctions, it is possible to restrict the calculations to k=0 in k space, and enlarge the unit cell instead. [12] It is common to most applications of these approaches that they restrict themselves to a slab consisting of two or several layers for the representation of the bulk, and this usually suffices to generate a good surface. Early studies by Kunz and co-workers [19] and by Clobourn and Mackrodt [20] used clusters terminated by full ionic charges and the choice of the appropriate charges for the point ions has been discussed for an fcc structure like MgO. [21] In the AIMP method, [22, 23] the metal oxide clusters are first embedded, then the rest of the crystal is taken to be full ionic charges. In the following two subsections, we will follow a procedure previously reported for metal oxides. [24, 25, 26]

Bulk simulation

A finite SrO crystal of 288 point charges was first constructed. The Coulomb potentials along the X and Y axes

Table 1 Specification of the finite lattices used for bulk, flat, edge and corner surfaces of SrO. *R* is half the lattice distance, which for SrO is 2.61 Å, and *r* is the distance of the appropriate shell from the center of the lattice

r^2/R^2	Bulk		Flat		Edge		Corner		Charge $\|q\|$
	Coordinates/*R* (±*X*), (±*Y*), (±*Z*)	Number of centers	Coordinates/*R* (±*X*), (±*Y*), (*Z*≤0)	Number of centers	Coordinates/*R* (±*X*), (*Y*≥–1), (*Z*≤0)	Number of centers	Coordinates/*R* (*X*≤1), (*Y*≥–1), (*Z*≤0)	Number of centers	
2	1 1 0	4	1 1 0	4	1 1 0	4	1 1 0	4	2
6	1 1 2	8	1 1 2	4	1 1 2	4	1 1 2	4	2
10	3 1 0	8	3 1 0	8	3 1 0	6	3 1 0	4	2
14	3 1 2	16	3 1 2	8	3 1 2	6	3 1 2	4	2
18	1 1 4	8	1 1 4	4	1 1 4	4	1 1 4	4	2
18	3 3 0	4	3 3 0	4	3 3 0	2	3 3 0	1	2
22	3 3 2	8	3 3 2	4	3 3 2	2	3 3 2	1	2
26	5 1 0	8	5 1 0	8	5 1 0	6	5 1 0	4	2
26	3 1 4	16	3 1 4	8	3 1 4	6	3 1 4	4	2
30	5 1 2	16	5 1 2	8	5 1 2	6	5 1 2	4	2
34	3 3 4	8	3 3 4	4	3 3 4	2	3 3 4	1	2
34	5 3 0	8	5 3 0	8	5 3 0	4	5 3 0	2	2
38	5 3 2	16	5 3 2	8	5 3 2	4	5 3 2	2	2
38	1 1 6	8	1 1 6	4	1 1 6	4	1 1 6	4	2
42	5 1 4	16	5 1 4	8	5 1 4	6	5 1 4	4	2
46	3 1 6	16	3 1 6	8	3 1 6	6	3 1 6	4	2
50	5 5 0	4	5 5 0	4	5 5 0	2	5 5 0	1	2
50	5 3 4	16	5 3 4	8	5 3 4	4	5 3 4	2	2
50	7 1 0	8	7 1 0	8	7 1 0	6	7 1 0	4	2
54	5 5 2	8	5 5 2	4	5 5 2	2	5 5 2	1	2
54	3 3 6	8	3 3 6	4	3 3 6	2	3 3 6	1	2
58	7 3 0	8	7 3 0	8	7 3 0	4	7 3 0	2	2
66	5 5 4	8	5 5 4	4	5 5 4	2	5 5 4	1	2
54	7 1 2	16	7 1 2	8	7 1 2	6	7 1 2	4	0.818566
62	7 3 2	16	7 3 2	8	7 3 2	4	7 3 2	2	0.818566
66	1 1 8	8	1 1 8	4	1 1 8	4	1 1 8	4	1.601818
82	9 1 0	8	9 1 0	8	9 1 0	6	9 1 0	4	1.601818
86	9 1 2	16	9 1 2	8	9 1 2	6	9 1 2	4	1.601818
		Σ=292		Σ=176		Σ=120		Σ=81	

of this crystal are zero by symmetry as in the host crystal. The ±2 charges on the outer shells listed in Table 1 were then modified, using a fitting procedure, to make the Coulomb potential at the four central sites closely approximate the Madelung potential of the host crystal, and to make the Coulomb potential at the eight points with coordinates (0,±*R*,±*R*) and (±*R*,0,±*R*) where *R* is half the lattice distance, which for SrO is 2.61 Å, equal to zero as it should be in the host crystal. With these charges, 0.818566 and 1.601818, the calculated Coulomb potentials in the region occupied by the central ions, ca. 3.496 for (0,±*R*,±*R*) and ca. 0.0 for (±*R*,0,±*R*), are very close to those in the unit cell of the host crystal, 3.496 for (0,±*R*,±*R*) and 0.0 for (±*R*,0,±*R*).

Surface simulation

The low coordinated surface sites of SrO crystal represented in Fig. 1 were generated as follows:

1. All charged centers with Cartesian coordinates (±*X*), (±*Y*) and (*Z*>0) were eliminated to generate a flat surface with 176 charged centers occupying the three dimensional space (±*X*), (±*Y*) and (*Z*≤0).
2. All charged centers with Cartesian coordinates (±*X*), (*Y*<–1) and (*Z*>0) were eliminated to generate an edge surface with 121 charged centers occupying the three dimensional space (±*X*), (*Y*≥–1) and (*Z*≤0).
3. All charged centers with Cartesian coordinates (*X*>1), (*Y*<–1) and (*Z*>0) were eliminated to generate the Br^- corner surface with 81 charged centers occupying the three dimensional space (*X*≤1), (*Y*≥–1) and (*Z*≤0).

The explicitly considered clusters of Fig. 2 were then embedded within the central region of the crystal surface. All the electrons of the embedded clusters were included in the Hamiltonian of the ab initio calculations. Other crystal sites entered the Hamiltonian either as full or partial ionic charges as demonstrated in Table 1.

Calculations

CC diagrams

The geometric relaxation of an F^+ center in the ground and excited states of an alkaline earth metal oxide is a key quantity for laser activity due to vibronic coupling. In other words, the possible energy level structure of an

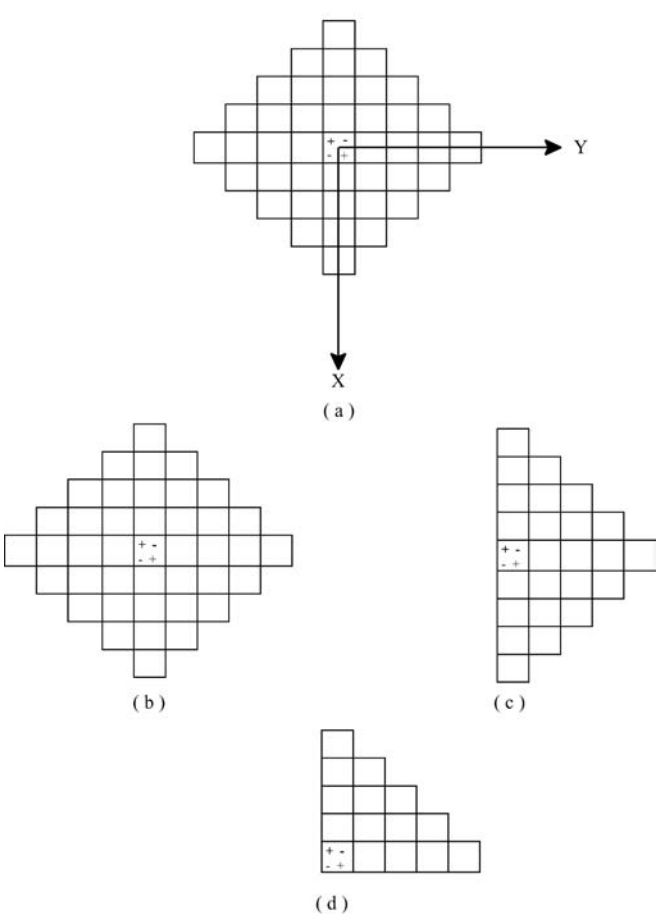

Fig. 1a–d Z=0 plane representation of the SrO crystal considered in the calculations. **a** Bulk. **b** Flat. **c** Edge. **d** Corner

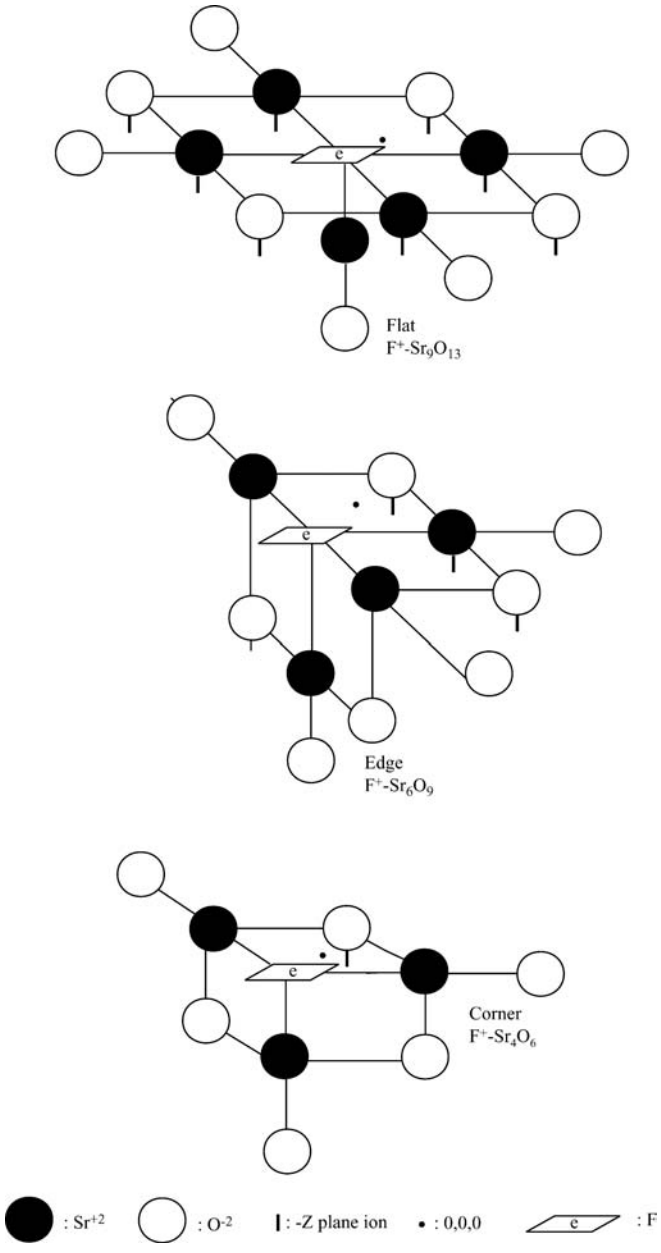

Fig. 2 The low coordinated surface clusters considered in the calculations

F^+ center electron is influenced by the shape and depth of the electronic binding potential. This potential is determined mainly by the distance and geometrical arrangement of the nearest surrounding lattice ions, which oscillate around their equilibrium positions. The ionic equilibrium is different for different electronic states and the electron–phonon coupling and its effect on the optical transitions can be illustrated with the configuration coordinate CC diagram. [27] In the CC diagram, the electronic energies in the ground and excited states are plotted against the displacement of usually a single configuration coordinate Q, which represents a certain localized mode or normal mode of the lattice coupling to the electron. This mode is sometimes called the linear coupling (bond breathing or symmetric stretching) mode. In other words, Q represents the simultaneous inward–outward displacements of the nearest neighbor cations to the defect site from the lattice interionic separation (Q=0.0) along the axes joining them with the defect site. The other ions were retained in their original positions in the lattice. Starting from the doublet ground state of an F_A center, an optical excitation produces a transition into the excited states at fixed nuclear coordinates assuming the Franck–Condon principle, i.e. vertical in the configuration coordinate diagram. Due to the Gaussian-shaped probability function for the lowest vibrational state, the transition starts with highest probability from the equilibrium position Q_1. The electronic distribution reached after excitation in the excited state is not in equilibrium with the lattice at Q_1. As a consequence, the ions oscillate towards a new equilibrium position. The vibrational energy will be dissipated via anharmonicity into lattice phonons and the electron–lattice system will reach the new equilibrium position Q_2, the relaxed excited state (RES). After the mean lifetime, the excited electron returns in a vertical emission process to the ground state,

and the subsequent lattice relaxation completes the optical cycle. [28]

To construct the CC diagrams, the ion clusters representing the F^+ centers at the flat, edge, and corner surfaces of SrO were first embedded in the three dimensional arrays of point ions described in the section Bulk simulation. The representation of the ion clusters considered in the calculations is given in Fig. 2. The absorption and emission energies were then calculated as the difference between the total energies of the ground and excited states. For this purpose the relevant potential energy curves were calculated, then according to the Franck–Condon principle the absorption energy was calculated as that for a vertical transition from the minimum of the relaxed ground state to the excited state (with fixed atomic coordinates). The luminescence energy was calculated in a similar manner. Stokes shifts were then calculated as the difference between absorption and emission energies.

$$\Delta E_{\text{absorption}} - \Delta E_{\text{emission}} \quad (1)$$

CI-Singles method

The CIS method was employed for the calculations of F^+ laser activity, exciton (energy) transfer, RES orientational destruction, and reorientational efficiency. Based on the formerly determined experimental geometry of SrO, partial geometry optimizations were carried out manually to obtain the equilibrium configurations of the ground and excited states. The CIS method, named CI-Singles, uses the configuration interaction approach and model excited states as combinations of single substitutions out of the Hartree–Fock ground state. The CI-Singles theory is an adequate zeroth-order treatment for many of the excited states of molecules. Treatments of large molecular systems can be afforded by the avoidance of integral storage and transformation, and thus the CI-Singles method has a wide range of applicability. A satisfactory exploration of potential energy surfaces and accurate electronic properties of excited states is possible by the use of an analytic CI-Singles gradient. [29, 30] The method can provide reasonable accuracy for excitation energies in comparison with the simplest way to find the lowest relaxed excited state in wide gap insulators, self consistent field calculations of the triplet state. [11]

DFT method

The density functional theory (DFT) method was employed for the calculations of F^+ relaxation and formation energies, the differences between the band gaps and exciton bands (Glasner–Tompkins relation), Mulliken charges, and adsorption energies. Based on the experimental geometry of SrO, partial geometry optimizations were carried out manually to obtain the adsorbate–substrate distances and energies. The DFT calculations were performed using Becke's three-parameter exchange functional B3 with LYP correlation functional. [31] This hybrid functional includes a mixture of a Hartree–Fock exchange with DFT exchange correlation. The functional B includes the Slater exchange along with corrections involving the gradient of the density. [32] The correlation functional LYP is that of Lee, Yang, and Parr, which includes both local and non-local terms. [33, 34]

CEP basis sets

The Stevens, Basch, and Krauss compact effective potential (CEP) basis sets were employed in the calculations. [35, 36, 37] In these pseudopotential basis sets, the double zeta calculations are referred to as CEP-31G and the triple zeta calculations are referred to as CEP-121G. However, there is only one CEP basis set defined beyond the second row elements, and the previous two basis sets are equivalent for these atoms. The CEP-121G basis set was employed in the present calculations. For the *s* manifold, a quadruple zeta representation of Gaussian type orbitals was found to be necessary to obtain energies within 0.001–0.003 a.u. of large, even-tempered basis set results. For this size expansion, little accuracy was lost by restricting the *s* and *p* basis sets for each atom to have a common set of expansions. For the *d* manifold, a three-GTO fit yields eigenfunctions, which are <0.001 a.u. different from large, even-tempered results. These potentials and basis sets have been used to calculate the equilibrium structure and spectroscopic properties of several molecules. All of the computations reported in this paper were carried out using the Gaussian 98 system. [38]

Results and discussion

$F^{\pm}$ laser oscillation and related properties

F^+ *laser oscillation*

The configuration coordinate data of F^+ centers at the low coordinated surfaces of SrO are given in Table 2 and the configuration coordinate curves are given in Fig. 3. The strength of the electron–phonon coupling as reflected by the shifts in the equilibrium positions Q_2–Q_1 and the values of Stokes shifts between the ground states and the lowest lying excited states suggest that F^+ laser oscillation fades quickly as the oxygen coordination decreases from 5 (flat) to 4 (edge) to 3 (corner), thus making the flat surface the most attractive compared with the edge and corner sites. The addition of oxygen basis functions to F^+ increased Stokes shifts, but the strength of the electron–phonon coupling was no longer reflected by the shifts in the equilibrium positions Q_2–Q_1.

The strong dependence of the absorption and emission energies, and consequently Stokes shifts, on ion coordination is probably due to the combination of several factors. Some have already been discussed by Garrone, Zecchina, and Stone [39] and include the reduction of

Table 2 Minima of the ground state (Q_1) the low lying excited state (Q_2), horizontal shifts along the configuration coordinate (Q_2–Q_1) for absorbed and emission transition energies ΔE between the ground state (g) and the excited state (e) of F^+ at SrO surface calculated at the CIS level. All lengths are given in Å and energies in eV. Lower figures in each case represent the data after adding O basis functions to F^+

	Q_1	Q_2	Q_2–Q_1	$\Delta E_{\text{absorption}}$ (g→e)	$\Delta E_{\text{emission}}$ (g←e)	Stokes shifts
Flat	0.360	0.433	0.073	0.857	0.319	0.538
	0.270	0.320	0.050	1.487	0.882	0.605
Edge	0.384	0.444	0.060	1.065	0.759	0.307
	0.300	0.350	0.050	1.360	0.961	0.399
Corner	0.423	0.448	0.026	0.712	0.606	0.106
	0.320	0.370	0.050	0.933	0.572	0.361

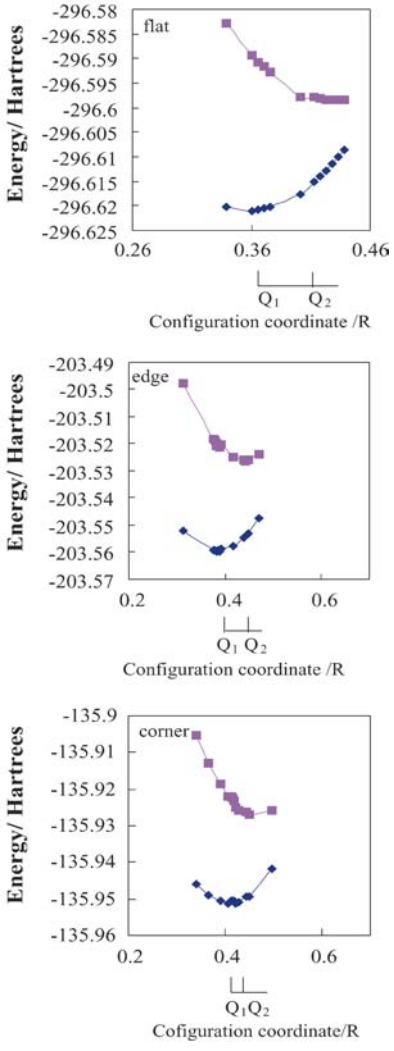

Fig. 3 The configuration coordinate diagrams of the low coordinated surfaces of Sr with F^+ center. Minima of the ground states (Q_1) and the low lying excited states (Q_2)

the Madelung potential at low coordinated sites, which leads to their substantial relaxation with respect to ideal geometry and to strong electron-density redistribution. However, the reduction of the Madelung potential alone cannot quantitatively explain the experimental data. This is perhaps not surprising because, as demonstrated in the calculations of Shluger et al., [40] both the degree of localization of the excited state and its nature depend on its location. Strong localization of the excited states on certain sites makes the Madelung argument less applicable.

Table 3 The tops of valence bands VB and the bottoms of conduction bands CB of the defect-free surfaces in the ground states and the HOMOs and LUMOs of the defect-containing surfaces in the relaxed excited states of the low coordinated surfaces of SrO. Energies are given in eV

	Defect-free surfaces ground states		Defect-containing surfaces relaxed excited states	
	VB	CB	HOMO	LUMO
Flat	–7.74	–1.46	–6.48	–3.82
Edge	–7.75	–1.44	–7.36	–4.04
Corner	–4.72	–0.81	–6.61	–3.27

With small Stokes shifts, the optical–optical conversion efficiency will be increased. On the other hand, the reabsorption of emitted light by other F^+ centers will also be increased. If the negative effect of reabsorption is stronger than the positive effect due to the conversion efficiency, then the laser activity will be decreased. Inspection of Table 2 reveals that the negative effect of reabsorption depends on surface coordination. In other words, the negative effect of reabsorption increases when one goes from the flat (5) to the edge (4) to the corner (3) surface.

A laser-suitable defect should have relaxed excited states deep below the conduction band of the perfect crystal. [5] To examine this issue, we consider the band structure of SrO surface, i.e. the positions of the one-electron defect levels with respect to the perfect surface bands. In Table 3, we present the tops of the valence bands (VB) and the bottoms of the conduction bands (CB) for the ground states of the defect-free surfaces as well as the highest occupied molecular orbitals (HOMOs) and the lowest unoccupied molecular orbitals (LUMOs) for the relaxed excited states of the defect-containing surfaces. As shown, all relaxed excited state defect level LUMOs are below the lower edges of the conduction bands of the defect-free surface's CB by ca. 2.36–2.46 eV, implying that F^+ is a laser-suitable defect.

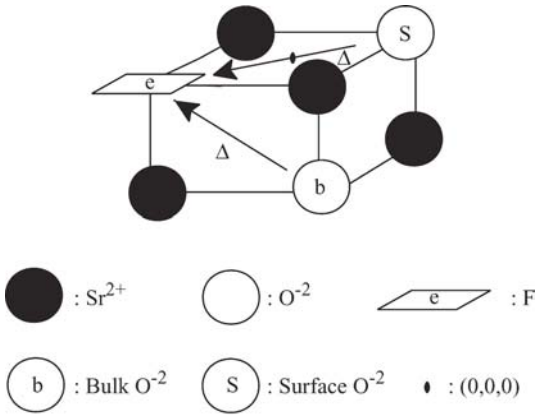

Fig. 4 Representation of the RES ion configurations responsible for orientational destruction of F^+ center at the low coordinated surfaces of SrO

RES orientational destruction

One consequence of the RES saddle point configuration of F^+ centers is a temperature-independent ionic reorientation during the pump cycle, i.e. a change of the center axis into a perpendicular (equivalent) orientation. A saddle point may be defined as a point at which a certain configuration has the maximum activation energy along a given path. The previous effect can be understood from Fig. 4, where it is seen that after the emission process the bulk or surface anion has a chance of hopping to the ⟨110⟩ anion vacancy site opposite its starting location. Therefore, if an F^+ center system is excited in either one of its absorption bands with polarized light having its propagation direction parallel to a ⟨100⟩ axis and the electric field vector E parallel to a perpendicular ⟨100⟩ axis, the F^+ centers excited by the E vector will quickly switch to ⟨100⟩ directions, where they are no longer excited and the system will become experimentally transparent for the excitation light. [5]

To examine the RES orientational destruction of F^+ theoretically, we calculated the total electronic energies of the original RES ion configuration (Δ=0.0) and the RES ion configurations obtained by moving one of the next nearest neighbor anions to the defect site along the ⟨110⟩ axis (Δ=0.25, 0.50, 0.75, and 1). In each case the nearest neighbor cations to the defect site were relaxed to equilibrium. The total electronic energies of the RES ion configurations as a function of the migration path Δ are given in Fig. 5. The differences between the energies of the original RES ion configuration and the RES saddle point ion configuration (the energy barriers to orientational destruction in laser experiment) are given in Table 4. As shown in Table 4 and Fig. 5, the orientational destruction of F^+ centers depends on the location of the anionic species as well as the surface coordination number. The destruction of F^+ by surface oxygen was easier than that by bulk oxygen, and while the flat surface was relatively the most probable surface for orientational destruction of F^+ by bulk oxygen, the corner surface was relatively the most probable surface for orientational destruction of F^+ by surface oxygen. Since the energy barrier to the migration of surface oxygen at the corner surface is smaller than the energy barrier to the migration of bulk oxygen at the flat surface, we may conclude that the least laser-active corner is fortunately the most probable site for orientational destruction of F^+. Experimentally, in order to avoid orientational destruction, the pump polarization and direction of propagation of the pump beam inside the crystal must be chosen such that they are not parallel to a ⟨100⟩ direction.

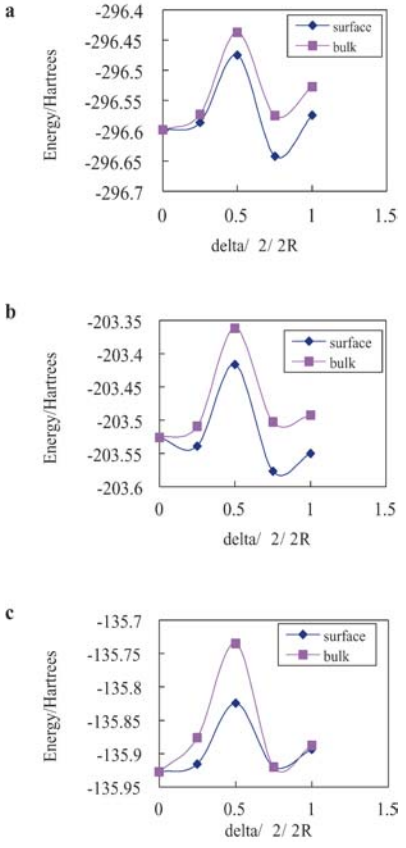

Fig. 5a–c The energetics of the RES orientational destruction of F^+ center at the low coordinated surfaces of SrO due to the migration of the bulk and surface anions along ⟨110⟩ axis. **a** Flat. **b** Edge. **c** corner

Table 4 The barrier heights of the RSE orientational destruction of F^+ center at the low coordinated surfaces of SrO due to the migration of the bulk and surface anions along the ⟨110⟩ axes. Energies are given in Hartrees

	Bulk O^{-2}	Surface O^{-2}
Flat	0.161	0.123
Edge	0.165	0.110
Corner	0.192	0.103

Reorientation efficiency and optical memories

It is possible to use the reorientation properties of defects under the action of polarized light to store information. [6] The reorientation efficiency is directly proportional to the recording sensitivity. Since the reorientation efficiency of the present F^+ center depends on surface coordination number, we may expect from Table 4 a relatively high recording sensitivity for the flat surface due to the migration of bulk oxygen, and for the corner surface due to the migration of surface oxygen. Since the energy barrier to the migration of surface oxygen at the corner surface is smaller than the energy barrier to the migration of bulk oxygen at the flat surface, we may expect the corner surface to give the maximum possible recording sensitivity.

Exciton (energy) transfer

Excitation transfer for vibronic materials was first formulated by Forster [41] and Dexter. [42] Orbach [43] discussed the factors affecting excitation transfer between ions in vibronic laser materials, gave examples of the important excitation transfer mechanisms, and introduced a new method for utilization of collision-induced electric-dipole radiation and collision-induced excitation transfer in the solid state.

The relative total energies of the excited states at different low coordinated surface sites could be used as the first indicator of whether the exciton excited at a particular surface site would transfer to another site. In order to be able to compare the results for different shapes and sizes of quantum clusters, the relative energies of the excited states for different coordinations were estimated following the method of Shluger et al. [11] The ionization energies I for the clusters were calculated using the CIS method. Assuming the vacuum level for all systems considered, the ground state total energies were placed at $-I$ as shown in Fig. 6. Then the energies of the excited states were located with respect to the defined positions of the ground states using the excitation energies. As can be seen from Fig. 6, the excited state at the edge site has the highest energy relative to the flat and corner sites. The excited state at the edge has higher energy than that at the flat surface, and the latter is higher than at the corner. In other words the relative energies at the low coordinated surfaces of SrO are sensitive to F^+ imperfections and there is a possibility for exciton transfer from the edge site to the other coordinated flat and corner sites. Cox and Williams [44] argued that the excited state at the surface is in the positive spectrum. Shluger et al. [11] suggested that it could have negative values for MgO. Our estimates suggest that it has only positive values for SrO, in agreement with the estimates of Cox and Williams.

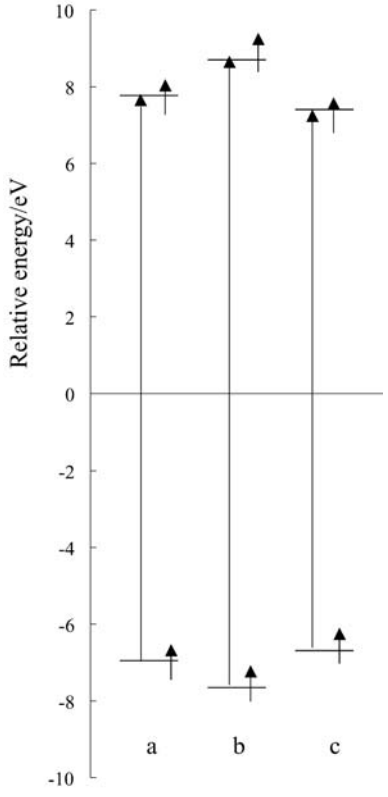

Fig. 6a–c Diagram representing the relative energies of the ground and excited states of the low coordinated surface sites of SrO using the CIS method. **a** Flat. **b** Edge. **c** Corner

Table 5 Equilibrium relaxation energies of the defect-containing surfaces of SrO calculated at the DFT level. Energies are given in eV

Flat	2.694
Edge	2.505
Corner	2.011

F^+ relaxation and formation energies

Since F^+ laser activity is related to surface coordination, an attempt has been made to calculate F^+ relaxation and formation energies at the low coordinated surfaces of SrO. Surface relaxation energies due to defect formation were calculated by subtracting the total electronic energy of the relaxed configuration (relaxed to equilibrium) from that of the unrelaxed configuration

$$\Delta E_{\text{relaxation}} = E_{\text{unelaxed}} - E_{\text{relaxed}} \quad (2)$$

Surface relaxation energies are given in Table 5, from which we conclude that surface relaxation energies decrease with decreasing surface coordination number. This means that the flat surface requires the largest amount of energy to relax to equilibrium.

Surface defect formation energies or defect creation probability were calculated by subtracting the sum of the total energies of the reactants from those of the products

$$\Delta E_{\text{formation}} = \sum E_{\text{products}} - \sum E_{\text{reactants}} \quad (3)$$

Table 6 The defect formation energies of SrO surface calculated at the DFT level. Energies are given in eV

Flat (Sr_9O_{14})→F^+-Sr_9O_{13}+O^-	12.096
Edge (Sr_6O_{10})→F^+-Sr_6O_9+O^-	10.867
Corner (Sr_4O_7)→F^+-Sr_4O_6+O^-	3.154

Here the reactants are the defect-free surfaces, and the products are the F^+ defect-containing surfaces (relaxed to equilibrium) and O^- anions. The defect-formation energies are given in Table 6, from which we conclude that F^+ defect-formation energies decrease with decreasing surface coordination number. This means that the most laser-active flat surface requires the largest amount of energy to create the F^+ center. In other words, the F^+ center at the most laser-active flat surface enjoys the largest continued stability, although it needs the largest amount of energy to relax to equilibrium.

The Glasner–Tompkins relation

Glasner and Tompkins [45] reported an empirical relationship between the principal optical absorption of *F* centers in solids and the fundamental absorption of the host crystal. The difference between the first exciton absorption energy E_X and the *F* band energy E_F was found to depend almost exclusively on the negative ion species. In other words, the Glasner–Tompkins empirical rule suggests that the energy difference between the fundamental absorption of an alkali halide and the *F* band is very nearly a function of the halide species alone. E_X, E_F, E_X–E_F, and $\langle E_X – E_F \rangle$ for 12 alkali halides have been reported by Malghani and Smith, [46, 47] and for LiH and LiF by Shalabi et al. [48] The dependence of the Glasner–Tompkins relation on the dopant cation and surface coordination number of MgO, KCl, and AgBr has also been reported by Shalabi et al. [49, 50, 51] Here we make an additional attempt to generalize this relation to include the low coordinated surfaces of SrO.

To apply the Glasner–Tompkins relation to the present F^+ center, we must calculate the corresponding band gaps and exciton bands. A complete treatment for understanding the host dependence of band gaps would involve theories of excitons [52, 53, 54] and defects [55, 56, 57, 58, 59] which take into account the band structure. Since this will be a major undertaking and well beyond our present goal, we will use the simple electron-transfer model of the fundamental optical absorption of ionic solids developed by Hilsch and Pohl. [60, 61] This model, in its simplest form, explains the fundamental optical absorption E_X as the transfer of an electron from a negative ion to a neighboring positive ion, both placed adjacent to the defect site. It seems likely that all color centers have perturbed excitons formed near them. [62, 63, 64, 65] We have therefore calculated E_X as the change in Coulomb energy, associated with the transfer of either one or two electrons E_{X1} and E_{X2} from an oxide anion to a neighboring strontium cation, both placed adjacent to the F^+ center, and calculate $E_F{}^+$ as the energy difference between the HOMO and LUMO energy levels. The correlation between the oxide-ion coordination, the F^+ center and the energy difference between the exciton bands E_{X1} and E_{X2}, and band gaps $E_F{}^+$ are given in Table 7. As one can see from Table 7, the results emphasize the dependence of the energy differences on the oxide coordination. The energy difference is reduced as the oxide ion coordination decreases, generalizing in turn the Glasner–Tompkins relation to include the surface coordination of SrO.

Table 7 F^+ band gaps $E_F{}^+$ and exciton bands E_{x1} and E_{x2} of the defect-containing surfaces of SrO calculated at the DFT level. Energies are given in eV

	$E_F{}^+$	E_{x1}	E_{x2}	E_{x1}–$E_F{}^+$	E_{x2}–$E_F{}^+$
Flat	0.849	30.96	46.59	30.11	45.75
Edge	1.002	30.24	45.09	29.24	44.09
Corner	1.000	28.13	41.15	27.13	40.15

The halogen–surface interactions

Electrostatic potentials

To shed light on the possible electrostatic contributions to the halogen–surface interactions of the defect-free and defect-containing surfaces, we calculated the electrostatic potential curves at the oxygen site of the defect-free surface and the F^+ site of the defect-containing surface. The electrostatic potential curves are shown in Fig. 7, from which we conclude that the electrostatic potentials due to the defect-free and defect-containing surfaces are very different for adsorbate–substrate interactions, thus leading to different electric fields and electric field derivatives. Since the electrostatic interaction of the adatom with the surface will consist mainly of electric field-induced dipole and electric field derivatives-induced quadrupole moments, one expects that the classical contributions to the adsorbate–substrate interactions are very different for the defect-free and defect-containing surfaces of SrO.

Adsorbate–substrate interactions

To examine the adsorbate–substrate interactions of the title halogens (F, Cl, and Br) under the effect of F^+ imperfection, we calculated the adsorption energies on two equivalent sites, the oxygen ion site of the defect-free surface and the F^+ site of the defect-containing surface, Fig. 8. The nearest and next nearest neighbor ions to the oxygen or F^+ site are considered in the calculations. The nearest neighbor ions to the F^+ site were first allowed to relax to equilibrium. The adsorbate–substrate distances were then optimized in each case. The corresponding results of the equilibrium adsorbate–substrate distances

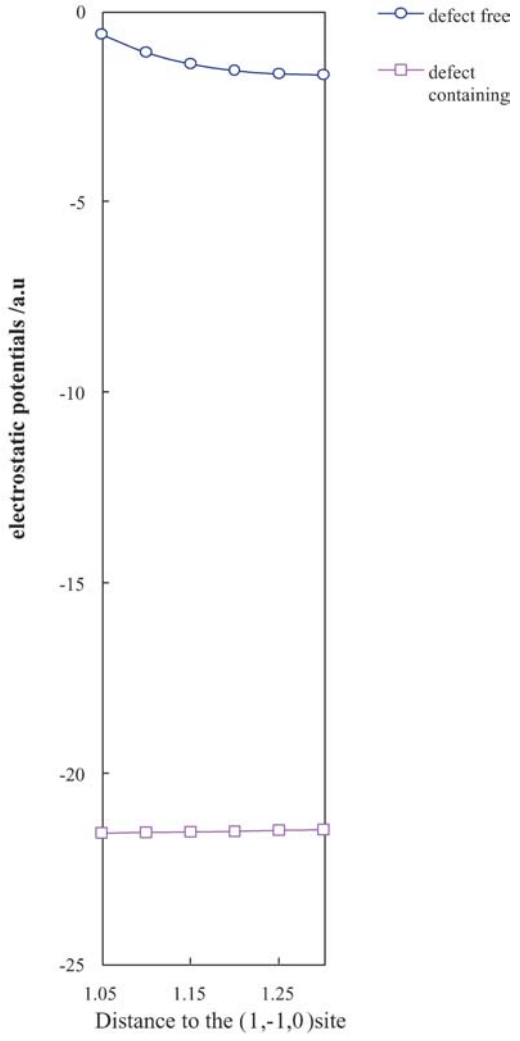

Fig. 7 The electrostatic potential curves of the defect-free Sr_9O_{14} and defect-containing F^+-Sr_9O_{13} surfaces of SrO

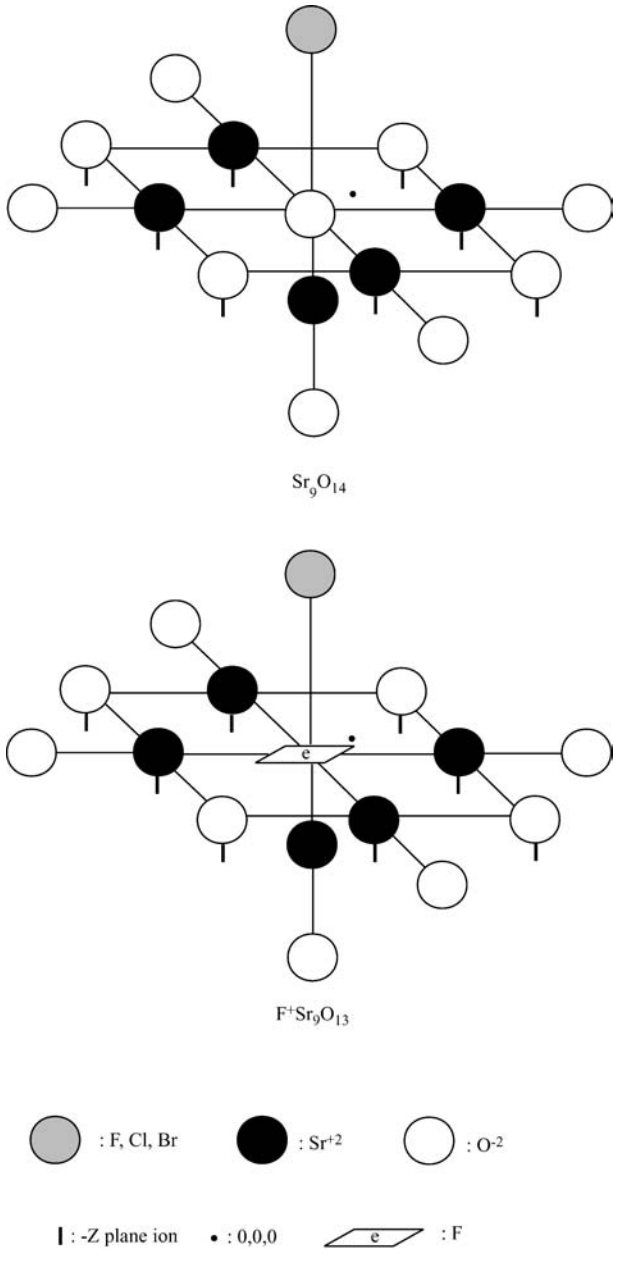

Fig. 8 The adsorption of F, Cl and Br over the defect-free (Sr_9O_{14}) and defect-containing (F^+-Sr_9O_{13}) surfaces of SrO

Table 8 Optimal adsorption energies $E_{ads.}$ and adsorbate-substrate distances R_e of F, Cl, and Br over the defect-free and defect-containing flat surfaces of SrO calculated at the DFT level. Energies are given in eV and distances in Å. The bottom figures refer to the data after adding O basis functions to F^+

	F		Cl		Br	
	R_e	E_{ads}	R_e	E_{ads}	R_e	E_{ads}
Sr_9O_{14}	2.2	0.835	2.5	1.514	2.5	1.851
F^+-Sr_9O_{13}	–0.2	–5.923	0.2	–3.790	1.2	–2.040
	0.0	–8.423	0.0	–6.900	1.0	–5.232

and interactions (adsorption energies) are collected in Table 8.

We may first note that the adsorption site over the oxygen atom is the energetically most favorable as confirmed by experimental data [66] and LDA-type calculations. [67, 68, 69, 70] Now, as shown in Table 8, the interaction energies of the considered halogens with the oxygen site of the defect-free surface were endothermic, while those with the F^+ site of the defect-containing surface were exothermic and the adsorbates were electronically stable. The F^+ center enhances the adsorption energies of halogens significantly and changes the nature of adsorption from physical adsorption to chemical adsorption, assuming a boundary value of ca.–1.5 eV between both types of adsorption. However, since there are no basis functions on F^+, the observed chemisorption may be due to a basis set superposition effect, as the basis set of the incoming halogen is used to stabilize the electron of the F^+ center. To test this point, oxygen basis functions were added to F^+ and the adsorption energies calculated.

As can be seen from the bottom figures of Table 8, the addition of an oxygen basis function enhanced the adsorption energies significantly, without altering the observed trend.

As shown in Table 8, the adsorption energies at the defect-free surface are endothermic ($+E_{ads.}$) while those at the defect-containing surface were exothermic ($-E_{ads}$). If we consider the adsorption energies to increase with increasing exothermicity ($-E_{ads}$) and/or decreasing endothermicity ($+E_{ads}$) the order of adsorption energies on both the defect-free and defect-containing surfaces should be essentially the same: F>Cl>Br, pointing to a dependence on the periodic properties of group VIIB halogens. While the calculated adsorption energy was directly proportional to the electronegativity of the halogen, the calculated adsorbate–substrate distance was inversely proportional, except for Cl and Br at the defect-free surface, where they were identical. The F atom penetrates the surface layer of the defect-containing surface and offers the maximum adsorbate–substrate interactions.

The significant increase in adsorption energies due to F^+ may be explained on the basis of spin pairing between the halogen single electron and the F^+ single electron. Here, the term "covalent spin pairing" may be suggested instead of "spin pairing" since the latter is based on the view of rigid two particles, while the former expresses the sense of smearing and overlapping. On the other hand, the pattern of adsorption energies is consistent with that expected from the electrostatic potential curves, where distinct differences in adsorption energies occur between the defect-free and the defect-containing surfaces.

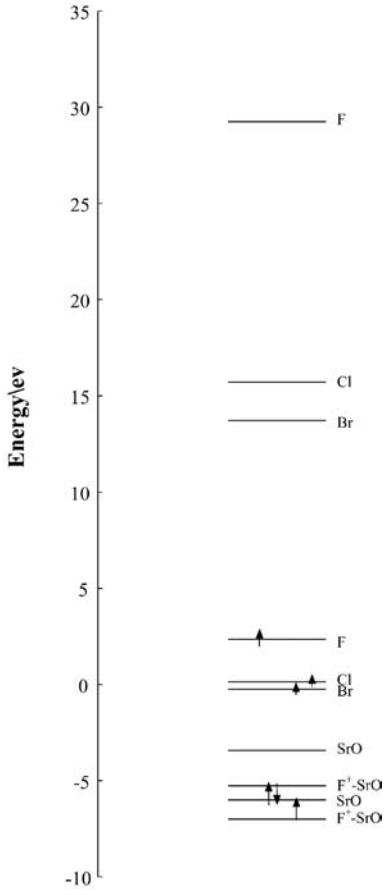

Fig. 9 HOMOs and LUMOs of the halogen atoms F, Cl, and Br; VB and CB of the defect-free surface (Sr_9O_{14}) and HOMO and LUMO of the defect-containing surface (F^+-Sr_9O_{13})

The roles of energy gaps and covalent spin pairing

To clarify the roles of (i) the energy gap between the adsorbate and the substrate, and (ii) the spin pairing between the adsorbate single electron and the substrate F^+ electron, in the course of adsorbate–substrate interactions, we calculated the highest occupied atomic orbital (HOAO) and the lowest unoccupied atomic orbital (LUAO) for each of the halogens considered, the top of the valence band (VB) and the bottom of the conduction band (CB) of the defect-free surface, and the highest occupied molecular orbital (HOMO) and the lowest unoccupied molecular orbital (LUMO) of the defect-containing surface. The calculated energy levels are shown in Fig. 9.

As shown in Fig. 9, covalent spin pairing is only allowed between the halogen and the defect-containing surface. The strength of adsorption follows the order F>Cl>Br despite the fact that the energy gaps between the HOAOs of the halogen atoms and the HOMO of the defect-containing surface increase from Br to Cl to F. This implies that covalent spin pairing, rather than the energy gap factor, plays the dominant role in the course of adsorbate–substrate interactions, and that the large increase in adsorption energies following surface imperfection is mainly attributed to the role of covalent spin pairing.

Band gaps and electrical conductivity

Figure 9 shows that the defect-free surface of SrO cannot be made semiconducting by F^+ imperfections. The band gap of the defect-free surface was not reduced to a value less than 2 eV, which is the domain of band gaps of semiconducting materials. However, the narrowing of band gaps suggests that the electrical conductivity of the insulator SrO can be enhanced under the effect of the F^+-trapped electron, in analogy with the behavior of the F-trapped electron in alkali hydrides and halides.

Conclusions

Ab initio molecular electronic structure calculations have been carried out to examine two practically important applications of F^+ (tunable laser activity and halogen–surface interactions) at the low coordinated surfaces

of SrO. Two commonly used methods, CIS and DFT, have been employed, and clusters of variable sizes ranging from 11 to 23 atoms have been embedded in simulated Coulomb fields of the low coordinated surfaces of SrO. Relaxation to equilibrium was taken into account and the CEP-121G basis set was used. Concerning the first application, the F^+ center was found to be laser active and the corresponding laser activity was dependent on the reduced oxygen coordination. Exciton (energy) transfer takes place from the edge to the flat and corner sites, and the Glasner–Tompkins relation is generalized to include the low coordinated surfaces of SrO. Concerning the second application, F^+ was found to change the nature of halogen–surface interaction from physical adsorption to chemical adsorption. A direct proportionality (or trend) exists between the strength of the halogen–surface interaction and the electronegativity of the halogen. The covalent spin pairing mode plays the dominant role relative to that of the energy gap in the course of the adsorbate–substrate interactions. We hope the present study stimulates further investigations of other twofold potential defects for more desirable properties of laser oscillation and surface adsorption.

References

1. Orbach R, Winter NW, Pitzer RM, Stoneham AM (1985) Tunable solid state lasers. In Hammerling LB, Budgor AB, Pinto A (eds) Proceedings of the First International Conference La Jolla, California, 13–15 June 1984. Springer Verlag Series in Optical Sciences, vol 47. Springer, Berlin Heidelberg New-York, pp 144–190
2. Seijo L, Barandiaran Z (1996) Int J Quantum Chem 60:617–634
3. Agullo-Lopez FA, Catlow CRA, Townsend PD (1988) Point defects in matrials. Academic Press, London, p 425
4. Shalabi AS, Nour ME, Morsi AM, Zordoc WA (2001) Curr Appl Phys 1:427–437
5. Gellermann W (1991) J Phys Chem Solids 52:249–297
6. Levine JD, Mark P (1966) Phys Rev 144:751–763
7. Garrone E, Zecchina A, Stone FS (1980) Philos Mag B 42:683–703
8. Kotomin EA, Kuklja MM, Eglitis RI, Popov AI (1996) Mater Sci Eng B37:212–214
9. Eglitis RI, Kulja MM, Kotomin EA, Stashans A, Popov AI (1996) Comput Mater Sci 5:298–308
10. Shluger AL, Catlow CRA, Grimes RW, Itoh N (1991) J Phys Condens Matter 3:8027–8036
11. Shluger AL, Sushko PV, Kantorovich LN (1999) Phys Rev B 59:2417–2430
12. Coluccia S, Marchese L (1988) In Tanabe K, Hattori H, Yamaguchi T, Tanaka T (eds) International Symposium on Acid–Base Catalysis. Kodansha, Tokyo
13. Finnis M (1996) J Phys Condens Matter 8:5811–5836
14. Stoneham AM, Ramos MMD, Sutton AP (1993) Philos Mag A 67:797–811
15. Henrich VE, Cox PA (1994) The surface science of metal oxides. Cambridge University Press, Cambridge
16. Goniakowski J (1999) Phys Rev B 59:11047–11052
17. Goniakowski J (1998) Phys Rev B 58:1189–1192
18. Heifets E, Zhukovskii YF, Kotomin EA, Causa M (1998) Chem Phys Lett 283:395–401
19. Surrat GT, Kunz AB (1978) Phys Rev Lett 40:347–350
20. Colbourn EA, Mackrodt WC (1982) Surf Sci 117:571–580
21. Colbourn EA (1999) In Catlow CRA (ed) Advances in solid state chemistry, vol I. JAI Press, London
22. Barandiaran Z, Seijo L (1988) J Chem Phys 89:5739–5746
23. Barandiaran Z, Seijo L (1992) Computational chemistry: structure, interactions and reactivity. In: Fraga S (ed) Studies in physical and theoretical chemistry, vol 77B. Elsevier, Amsterdam, pp 435–481
24. Shalabi AS, El-Mahdy AM (2001) Phys Lett A 281:176–186
25. Shalabi AS, El-Mahdy AM (1999) J Phys Chem Solids 60:305–315
26. Shalabi AS, El-Mahdy AM (1998) J Phys Chem Solids 59:395–401
27. Fowler WB, Dexter DL (1965) Chem Phys 43:1768–1771
28. Luty F (1968) In: Fowler WB (ed) Physics of color centers, Chap 3. Academic Press, New York
29. Foresman JB, Head-Gordon M, Pople JA, Frisch MJ (1992) J Phys Chem 96:135–149
30. Foresman JB (1996) Exploring chemistry with electronic structure methods, 2nd edn. Gaussian, Pittsburgh, Pa. p 213
31. Becke AD (1993) J Chem Phys 98:5648–5652
32. Becke AD (1988) Phys Rev A 38:3098–3100
33. Lee C, Yang W, Parr RG (1988) Phys Rev B 37:785–789
34. Miehlich B, Savin A, Stoll H, Preuss H (1989) Chem Phys Lett 157:200–206
35. a) Stevens W, Basch H, Krauss J (1984) J Chem Phys 81:6026–6033
36. Stevens W, Krauss M, Basch H, Jasien PG (1992) Can J Chem 70:612–630
37. Cundari TR, Stevens WJ (1993) J Chem Phys 98:5555–5565
38. Frisch MJ, Trucks GW, Schlegel HB, Scuseria GE, Robb MA, Cheeseman JR, Zakrzewski VG, Montgomery JA, Stratman RE, Burant JC, Dapprich S, Millam JM, Daniels AD, Kudin KN, Strain MC, Farkas O, Tomasi J, Barone V, Cossi M, Cammi R, Mennucci B, Pomelli C, Adamo C, Clifford S, Ochterski J, Petersson GA, Ayala PY, Cui Q, Morokuma K, Malick DK, Rabuck AD, Raghavachari K, Foresman JB, Cioslowski J, Ortiz JV, Baboul AG, Stefanov BB, Liu C, Liashenko A, Piskorz P, Komaromi, I, Gomperts R, Martin RL, Fox DJ, Keith T, Al-Laham MA, Peng CY, Nanayakkara A, Gonzalez C, Challacombe M, Gill PMW, Johnson BG, Chen W, Wong MW, Andres JL, Gonzales C, Head-Gordon M, Replogle ES, Pople JA (1998) Gaussian 98. Gaussian, Pittsburgh Pa.
39. Garrone E, Zecchina A, Stone FS (1980) Philos Mag B 42:683–703
40. Fitchen DB (1968) In: Fowler WB (ed) Physics of color centers, Chap 5. Academic Press, New York
41. Forster T (1948) Ann Phys 2:55–75
42. Dex DL (1953) J Chem Phys 21:836
43. Orbach R (1985) Energy transfer in vibronic laser materials. In: Hammerling P, Budgor AB, Pinto A (eds) Tunable solid state lasers. Springer, Berlin Heidelberg New York, pp 144–154
44. Cox PA, Williams AA (1986) Surf Sci 175:L782-L786
45. Glasner A, Tompkins FC (1953) J Chem Phys 21:1817–1818
46. Malghani MS, Smith DY (1991) Bull Am Phys Soc 36:1681
47. Malghani MS, Smith DY (1992) J Phys Chem Solids 53:831–840
48. Shalabi AS, El-Mahdy A, Eid KM, Kamel MA, El-Barbary AA (1999) Phys Rev B 60:9377–9382
49. Shalabi AS, El-Essawy TF, Assem MM, Abdel-Aal S, El-Mahdy AM (2002) J Phys Chem Solids 63:749–758
50. Shalabi AS, El-Essawy TF, Assem MM, Abdel-Aal S, El-Mahdy AM (2002) Curr Appl Phys 2:97–105
51. Shalabi AS, El-Essawy TF, Assem MM, Abdel-Aal S, El-Mahdy AM (2002) Physica B 315:13–28
52. Knox RS (1963) Theory of excitons. Academic Press, New York
53. Plekhanov VG (1996) Phys Rev B 54:3869–3877
54. Connel-Bronin AAO (1996) Phys Status Sol 38:1489
55. Koster GF, Slater JC (1954) Phys Rev 95:1167
56. Koster GF, Slater JC (1954) Phys Rev 96:1208–1223
57. Crawford JH, Slifkin LM (1972) Point defects in solids. Plenum, New York
58. Hayes W, Stoneham AA (1985) Defects and defect processes in non-metallic solids. Wiley, New York

59. Kotomin E, Popov A (1998) Nucl Instrum Methods B 141:1–15 and references cited therein
60. Hilsch R, Pohl RW (1929) Z Phys 57:145–153
61. Hilsch R, Pohl RW (1929) Z Phys 59:812–819
62. Shalabi AS, El-Mahdy AM, Kamel MA, Ammar HY (2000) Phys B 292:59–70
63. Shalabi AS, Eid KM, Kamel MA, Fathi ZM (2000) Int J Mod Phys C 11:1491–1507
64. Shalabi AS, El-Mahdy AM, Kamel MA, Ismail GH (2001) J Phys Chem Solids 62:1007–1013
65. Shalabi AS, El-Mahdy AM, Kamel MA, Ammar HY (2001) Phys B 304:444–455
66. Ernest F (1995) Mater Sci Eng R14:97
67. Schonberger U, Andersen OK, Methfessel M (1992) Acta Metall Mater Suppl 40:1–10
68. Li C, Wu R, Freeman AJ, Fu CL (1993) Phys Rev B 48:8317–8322
69. Smith JR, Hong T, Srolovich DJ (1994) Phys Rev Lett 72:4021–4024
70. Hong T, Smith JR, Srolovich DJ (1995) Acta Metall Mater 43:2721–2730